

## MIT Open Access Articles

*Mechanical and thermal performance of aerogel-filled sandwich panels for building insulation*

The MIT Faculty has made this article openly available. **Please share** how this access benefits you. Your story matters.

**Citation:** Chen, K., A. Neugebauer, T. Goutierre, A. Tang, L. Glicksman, and L.J. Gibson. "Mechanical and thermal performance of aerogel-filled sandwich panels for building insulation." *Energy and Buildings* 76 (June 2014), pp. 336-346.

**As Published:** <http://dx.doi.org/10.1016/j.enbuild.2014.02.041>

**Publisher:** Elsevier

**Persistent URL:** <http://hdl.handle.net/1721.1/103944>

**Version:** Author's final manuscript: final author's manuscript post peer review, without publisher's formatting or copy editing

**Terms of use:** Creative Commons Attribution-NonCommercial-NoDerivs License



# **Mechanical and Thermal Performance of Aerogel-Filled Sandwich Panels for Building Insulation**

Chen K,<sup>1</sup> Neugebauer A,<sup>2</sup> Goutierre T,<sup>1</sup> Tang A,<sup>3</sup> Glicksman L<sup>2</sup> and Gibson LJ<sup>3</sup>

<sup>1</sup>Department of Mechanical Engineering

<sup>2</sup>Department of Architecture

<sup>3</sup>Department of Materials Science and Engineering

Massachusetts Institute of Technology

Cambridge MA 02139

## **Corresponding Author**

Lorna J. Gibson

1-617-253-7107

[ljgibson@mit.edu](mailto:ljgibson@mit.edu)

77 Massachusetts Avenue

Building 8, Room 135

Cambridge, MA 02139

## **Abstract**

Monolithic silica aerogels have exceptional thermal insulation but low mechanical properties. For instance, their flexural strength is typically 0.03-0.08 MPa. Here, we report on the development of a truss-core sandwich panel filled with compacted aerogel granules, designed to provide both mechanical support and thermal insulation. Mechanical and thermal properties of the sandwich panel prototype were measured and compared with theoretical models available in the literature. The models give a good description of the properties of aerogel-filled truss-core sandwich panels.

## **Keywords**

Mechanical characterization; strain measurement; polymers; bonding; failure; fracture

## Introduction

Space heating and cooling in commercial and residential buildings consumed 15.6% of the energy used in the United States in 2011 [1]. Energy consumption, as well as greenhouse gas emissions, can be reduced by the use of high performance insulation materials and products. Aerogels, with their exceptionally low thermal conductivity of 9-17 mW/(m·K) (compared to 25 mW/(m·K) for conventional closed-cell polyurethane foams [2] and 40 mW/(m·K) for standard fiberglass batts [3]), offer great potential for improving insulation of buildings and reducing energy consumption [4, 5].

The weak and brittle nature of monolithic aerogels makes them impractical for use in building insulation, however. Currently available commercial aerogel products use granules: for instance, in a fiber mat or as blown insulation in cavity walls. Granular aerogel has a higher thermal conductivity than monolithic aerogel, due to the higher conductivity air (25 mW/(m·K)) between the granules. In a previous study in our group, the contribution of air to the thermal conductivity of granular aerogel was minimized by physically compacting the granules together. We showed that the thermal conductivity of compacted granular silica aerogels can be reduced to 13 mW/(m·K), nearly half the value of the uncompact granules [6].

Here, we report on the development of a truss-core sandwich panel filled with compacted aerogel granules, designed to provide both mechanical support and thermal insulation. One potential application for such panels is as interior insulation, retrofit to existing buildings. Sandwich structures are particularly attractive as the separation of the faces by the lightweight core increases their moment of inertia, making them mechanically efficient in resisting bending loads encountered in handling and transporting the panels. Truss cores are preferred over conventional honeycomb cores since, for a given material and core thermal conductivity, they

have higher shear and compressive strengths. The design of such a structure must also consider the contribution of the sandwich core to the overall thermal conductivity of the panel.

In this study, the uniaxial compression and bending response of a truss-core sandwich panel are measured and compared with theoretical models available in the literature. The thermal conductivity of the panel filled with compacted granular silica aerogel is also measured and compared with previous results for the compacted granular aerogel.

## **Materials and Methods**

### *Sandwich Panel Material*

To demonstrate the feasibility of a truss core sandwich panel filled with compacted granular aerogel, solid polystyrene (McMaster-Carr, Robbinsville, NJ) was chosen as the material for the sandwich panel as it combines high Young's modulus and tensile strength with relatively low thermal conductivity and cost per unit volume, compared with other polymers. Of potential materials with a high ratio of Young's modulus to thermal conductivity, ( $E/\lambda$ ), identified using a material selection chart [7], polystyrene is the most readily accessible and easiest to machine. For materials with similar  $E/\lambda$  values, the material with the lower thermal conductivity is preferred.

The uniaxial tensile stress-strain response of the polystyrene sheet was measured on 5 dogbone specimens in an Instron testing machine (Instron Model 4201, Canton, MA). The dogbones were cut both using a water jet cutter (OMAX Model 2626, Kent, WA) and a laser cutter (Universal Laser Systems V460, Scottsdale, AZ), to determine if the mechanical properties of the material are affected by the thermal treatment due to the laser. The waisted section of the dogbones was 57 mm long, 13 mm wide and 2 mm thick [8]. Displacement was measured with

an extensometer (Instron Model 2630-033, Canton, MA) attached to the waisted section of the dogbone. The uniaxial compressive stress-strain response was measured on 5 small laser-cut rectangular prisms of the polystyrene sheet 4 mm long, 2 mm wide and 2 mm thick. Displacement was measured using the crosshead displacement of the Instron.

### *Aerogel*

Silica-based P100 series granular aerogels were purchased from Cabot Corporation (Boston, MA). Particle sizes range from 0.01 to 4 mm, with a density between 120 and 180 kg/m<sup>3</sup> [9]. Aerogels are typically made by mixing a precursor material, such as tetraethoxysilane (TEOS) or tetramethoxysilane (TMOS), with other chemicals, such as ethanol, to hydrolyze and polymerize the silica, resulting in a sol-gel. The solution is then supercritically dried in a chamber, such as an autoclave, to remove the liquid from the sol-gel. The chamber is heated and pressurized until the fluids reach a supercritical phase, and are freely mobile without creating surface tension. The critical point for ethanol is 241°C at 6.3 MPa, which is a dangerous condition for flammable material like ethanol. Therefore, for this process, the ethanol is typically replaced with supercritical carbon dioxide (the critical point for carbon dioxide is 31°C at 7.4 MPa) by solvent exchange. After the solvent exchange is complete, the material is slowly brought back down to atmospheric pressure, resulting in aerogel. (Room temperature evaporation is avoided as the resulting surface tension and capillary forces can damage the fragile microstructure of the material.)

### *Panel Design*

Various truss-core geometries were considered for the panel: regular tetrahedra, tetrahedra with struts at a 45° angle to the vertical, and pyramids. All three core configurations

had the same thermal conductivity for a given relative density, based on a one dimensional conduction analysis of the cores. The relative density of the truss core was selected to limit the contribution of the core to the thermal conductivity of the panel to 2 mW/(m·K). The pyramidal truss lattice structure was ultimately selected since this geometry lent itself to fast prototype fabrication. The method of truss core fabrication was inspired by the work of Finnegan and co-workers [10].

### *Panel Fabrication*

Two-dimensional truss segments were cut from a 1.6 mm thick sheet of polystyrene using a laser cutter to give a square strut cross section (Fig. 1a). Segments were then assembled into the 3D truss core (Fig. 1b). The truss patterns were designed with mechanical snap fits at the location of the nodes, to facilitate assembly and secure the lattice. Once the core of the panel was created, it was joined to 2 mm thick polystyrene face sheets using a fast-setting epoxy (ITW Devcon, 5 Minute® Epoxy, Danvers MA); the face sheet thickness was chosen to be higher than that of the core trusses to avoid face sheet failure. The manufacturer's reported value of the adhesive shear strength was 13.1 MPa [11]. Adhesive was placed on the nodes formed at the junctions between orthogonal truss segments; the epoxy was allowed to set and cure for 24 hours. The unit cell of the truss core is shown schematically in Fig. 2; the dimensions of the panel are listed in Table 1. A typical panel specimen used in the mechanical tests is shown in Fig. 3a.

### *Introduction and Compaction of Granular Aerogel*

For the thermal conductivity tests, the voids between the trusses in the panel were filled with granular aerogel. To contain the particles, polystyrene sidewalls were connected to the panel faces. Each sidewall was in two pieces: the lower piece was fixed to the bottom plate while the upper piece was temporary, to allow the granules to be compressed into the voids between the trusses (Fig. 3b). Once the granules were compacted into place using a custom fixture, with slots corresponding to the lines of the trusses, the upper piece was removed and the top face of the sandwich was bonded to the lower side piece and the trusses (Fig. 3c).

Uncompacted aerogel granule beds had an initial density of roughly  $68 \text{ kg/m}^3$ . We mechanically compacted the granules into the panel prototypes, increasing the average bed density across the panel to approximately  $95 \text{ kg/m}^3$ , or a compressive strain of 30%. The compression platen was designed to fit around the truss structure, effectively pressing 58% of the surface area. The compressive strain value corresponds to the maximum compaction we were able to achieve in a previous study; compaction was limited by elastic rebound [6].

### *Mechanical Tests*

Four truss core specimens were tested in shear using specimens 15 mm thick, 74 mm wide and 252 mm long, designed according to ASTM Standard C273 [12]. Each truss core specimen was attached to two loading plates on either side of the specimen via tabs that extended beyond the nodes of the truss lattice and that passed through holes machined into the loading plates; the tabs were held in place using epoxy. This setup was developed to avoid adhesive failure, which occurred in initial tests with the core bonded directly to the surface of the loading plates. Displacement between the two plates was measured using an LVDT. The shear tests were performed at a rate of 0.5 mm/minute.

The sandwich panels (without the granular aerogel or the side walls) were subjected to uniaxial compression, plate bending under a uniformly distributed load and plate bending under an approximately concentrated load. The sandwich panels were square, with edge length 159 mm.

Uniaxial compression tests on four sandwich panels were performed in an Instron machine (Instron Model 1321, Canton, MA), with the platens of the machine parallel to the faces of the panel. Each panel was compressed at a displacement rate of 1 mm/minute until failure; displacement was recorded using the crosshead displacement.

Plate bending tests were performed on square specimens, with the edges of the panel resting on a 12.5 mm wide square frame supporting the outer edge of the specimen. The unsupported edge length of each panel,  $b$ , is 139 mm. The displacement of the center of the panel was measured using a LVDT beneath the panel. For the uniformly distributed loading, a 12.5 mm thick layer of rubber, the same size as the unsupported area of the panel, was attached to the upper compression platen. This ensured that as the panel bent, there would be constant contact between the fixture and the panel, as the rubber would be able to conform to the resulting curvature of the panel face. The setup for plate bending under an approximately concentrated load was similar to that of the uniformly distributed load except that the approximately concentrated load was applied by a cylindrical fixture, with a radius of 15.9 mm. Four specimens were tested for each type of plate bending loading.

#### *Thermal Conductivity Tests*

The thermal conductivity of the panels was measured using the steady state hot-plate method (LaserComp FOX304, Saugus, MA). The thermal conductivity is evaluated by placing



the sample between two parallel plates that are held at constant temperatures with a set temperature differential between them. Once the system reaches thermal equilibrium, the conductivity of the sample can be calculated using Fourier's Law. The heat flux flowing through the system from the hot plate to the cold plate is determined based on the energy required to hold the plates at constant temperature. The LaserComp system is a center-of-panel design (i.e., the heat flow measurements are taken from a 10.2 by 10.2 cm metering area in the center of the chamber), so the impacts of the edge pieces of the insulation panels can be ignored.

A variety of panel configurations were tested with the LaserComp system. These include panels with uncompacted aerogel beds with and without a truss, panels of compacted aerogel beds with and without a truss, panels of compacted aerogels made by both holding the granules at a fixed level of compression and by cyclically loading and unloading them, and panels of compacted aerogels made by both applying an adhesive to the entire face between the face sheet and truss core and applying an adhesive to only the contact points between the face sheet and truss core. The thermal conductivity testing was done on square panels of edge length 247 mm, with outer walls between the face sheets to contain the aerogel granules. One sample was tested for each configuration.

The LaserComp testing method gives the thermal conductivity of the sample as if it was one homogeneous material, according to Fourier's Law:

$$k_s = \frac{t_s Q_{ss}}{A_s (T_H - T_C)} \quad (1)$$

Here,  $k_s$  is the thermal conductivity of the sample,  $t_s$  is the sample thickness (in our case, the thickness of the panel, including the two face sheets),  $Q_{ss}$  is the energy flux through the sample at steady state,  $A_s$  is the cross-sectional area of the sample normal to the heat flow, and  $T_H$  and  $T_C$  are the steady state temperature of the hot plate and cold plate, respectively. It should be

noted that the LaserComp system measures one dimensional heat flow through the panel system, with the panel core in series with the two panel faces, and only the center-of-panel thermal conductivity. The edge effects of the insulation panels due to the presence of the polystyrene walls are therefore absent from the measured value. A schematic representation of the heat flow through the panel is shown in Fig. 4. The thermal conductivity of the aerogel in the core of the panel can be obtained from the measured whole-panel conductivity by representing the sample as a thermal resistance network. The current analysis ignores multidimensional heat transfer between the truss elements and the panel faces. In the conductivity tests, the outer surface of the each panel face is in contact with constant temperature plates. The true truss-end plate heat transfer lies between two limits: negligible lateral conduction in the end plate and infinite lateral conductivity of the end plate. In the former, heat flow from the truss end is confined to an equal cross section as it passes through the thickness of the end plate. In the latter limit, the truss and core are in series with the entire end plate. The difference in the overall assembly heat transfer is only three percent in the two limits; thus the latter assumption was adopted with little loss of accuracy. Using this model the conductivity of the sample can be derived as,

$$\frac{t_s}{k_s} = \frac{2t_f}{k_f} + \left( \frac{A_a}{A_c} \frac{k_a}{h} + \frac{A_t}{A_c} \frac{k_t}{L_t} \right)^{-1} \quad (2)$$

$$k_a = \frac{h}{A_a} \left[ A_c \left( \frac{t_s}{k_s} - \frac{2t_f}{k_f} \right)^{-1} - A_t \frac{k_t}{L_t} \right] \quad (3)$$

Here  $k_a$  is the thermal conductivity of the aerogel in the panel core,  $k_t$  is the thermal conductivity of the truss material and  $k_f$  is the thermal conductivity of the facing material;  $h$  is the thickness of the core,  $t_f$  is the thickness of a single panel facing and  $L_t$  is the length of a truss segment;  $A_c$  is the cross-sectional area of the panel core,  $A_a$  is the total cross-sectional area of the

aerogel and  $A_t$  is the total cross-sectional area of the truss. All of these cross-sectional areas are measured normal to the heat flow through their respective components.

This relationship can be further simplified according to the specific design used for our testing. First, the truss and panel faces were made from the same material, so  $k_t$  equals  $k_f$ . Then, according to the truss geometry,  $L_t$  is equal to  $h/\sin \omega$ , where  $\omega$  is the angle between the panel face and the truss segments. Similarly,  $A_t$  can be represented as  $A'_t \sin \omega$ , such that  $A_c$  is simply the sum of  $A_a$  and  $A'_t$ . Therefore, eqn 3 can be rewritten as:

$$k_a(\text{with truss}) = \frac{t_s - 2t_f}{\phi_a} \left( \frac{t_s}{k_s} - \frac{2t_f}{k_f} \right)^{-1} - \left( \frac{1}{\phi_a} - 1 \right) k_f \sin^2 \omega \quad (4)$$

Here,  $\phi_a$  is the volume fraction of aerogel in the core (which is equal to  $A_a/A_c$  or  $1 - A'_t/A_c$ ).

This assumes that the truss and the aerogel make up the entire volume of the core and that the thickness of the core is equal to that of the whole panel minus the two panel face layers. For the case of our  $45^\circ$  truss,  $\sin^2 \omega$  equals 0.5. Also, for the case where there panels were tested with no internal truss, eqn 4 simplifies to:

$$k_a(\text{without truss}) = (t_s - 2t_f) \left( \frac{t_s}{k_s} - \frac{2t_f}{k_f} \right)^{-1} \quad (5)$$

It is also worth noting that the contribution of the truss system to the thermal conductivity of the whole panel,  $k'_t$ , can be represented as:

$$k'_t = (\phi_t \sin^2 \omega) k_t \quad (6)$$

Here,  $\phi_t$  is the volume fraction of truss in the core (which is equal to  $A'_t/A_c$  or  $1 - \phi_a$ ).

Additional hot-plate tests were required to determine an accurate value for the conductivity of the polystyrene used for the face sheets and trusses, as this was not available

from the manufacturer. Literature values for the thermal conductivity of solid polystyrene were between 126 and 150 mW/(m·K) [13, 14]. The thermal conductivity of a stack of five sheets was measured to be 112 mW/(m·K). The test set-up could not accurately measure the conductivity of a single sheet and the manufacturer of the polystyrene sheets did not offer thick blocks of the exact same material, so stacks of sheets were tested in order to measure the conductivity of the polystyrene. However, this measurement is influenced by the contact resistances in the spatial gaps between the sheets (Fig. 5), which are not readily quantifiable; additionally, the test set-up did not allow for increased compression of the sample to minimize the contact resistances. Attempts to minimize these resistances with a high conductivity thermal paste were unsuccessful. For future research details of a methodology used to find a more accurate conductivity value for the polystyrene sheets is available in the Appendix.

## Results

### *Uniaxial Tests on Polystyrene Sheet*

The uniaxial tensile and compressive stress strain responses of the polystyrene sheet, cut using a laser cutter, are shown in Fig. 6. The Young's modulus and ultimate tensile strength, corresponding to the peak load, are  $1.60 \pm 0.28$  GPa and  $15.4 \pm 0.31$  MPa, respectively. We note that earlier tests, on dogbones made using a water-jet cutter, gave similar values of modulus and tensile yield strength, but were considerably more ductile, deforming to strains of over 25% at failure (data not shown). The use of the water jet was discontinued, as individual truss segments were frequently lost in the water jet cutting process. The 0.2% offset compressive strength was  $35.5 \pm 0.39$  MPa.

### *Shearing of Truss-Core*

A typical stress-strain curve of the truss core specimens tested in shear is plotted in Fig. 7. The curves are initially linear elastic up until yielding. After initial yielding, the slopes of the stress strain curves gradually decrease; in this region a few instances of audible cracking occurred, although no noticeable changes were visible in the structure. The curves peak at an ultimate shear stress of  $0.12 \pm 0.01$  MPa, at which point the specimens began to exhibit cracks near the nodes of the tensile truss members. As the test progresses, existing cracks grow and new cracks appear in the same location on more members; the stress gradually decreases until the specimen fractures (Fig. 8).

The shear modulus of the core is  $8.32 \pm 1.71$  MPa, slightly above the value of 6.51 MPa (eqn A4d) predicted by Queheillalt and Wadley [15], who modified the previous derivation of Deshpande and Fleck [16]. The 0.2% offset shear strength of the core is  $0.084 \pm 0.007$  MPa.

The struts in a pyramidal truss core loaded in shear can fail by uniaxial tensile or compressive yield, elastic Euler buckling or plastic buckling; each of these failure modes has been analyzed by Deshpande and Fleck [16], modified slightly by Queheillalt and Wadley [15] to account for the material at the nodes in fabricated truss cores. For the polystyrene struts in this study, the tensile yield strength is less than half the compressive; uniaxial ultimate tensile yield is calculated to occur at a core shear stress  $\tau_{\text{uniaxial yield}}^* = 0.18$  MPa (eqn A8), and was the only mode of failure present in the experiments. The results of the truss-core shearing tests are summarized in Table 2.

### *Uniaxial Compression of Truss-Core Sandwich Panels*

The stress-strain curves of the truss-core sandwich panels under uniaxial compression are shown in Fig. 9. The curves show an initial toe (associated with a slight non-parallel misalignment of the top and bottom faces of the panel), followed by a linear elastic regime up to a peak stress. Immediately following the peak stress, there is a sharp drop in stress, to about half the peak value, followed by a more gradual decline in stress. The truss core was observed to fail by plastic buckling, followed by debonding (Fig. 10).

The compressive Young's modulus of the panel is  $15.1 \pm 0.9$  MPa, slightly higher than the theoretical value of 13 MPa calculated from the model of Queheillalt and Wadley [15] (eqn A1), who modified the earlier result of Deshpande and Fleck [16].

The measured peak compressive strength, corresponding to failure by plastic buckling, is  $0.50 \pm 0.02$  MPa. The uniaxial compressive failure of truss cores has been analyzed for both plastic yielding (eqn A2) and elastic buckling (eqn A3) using the results of Queheillalt and Wadley [15], who slightly modified the earlier results of Deshpande and Fleck [16]. Yielding is predicted to occur at a uniaxial compressive stress of 0.58 MPa, slightly above the measured failure stress associated with plastic buckling. Elastic buckling, assuming the ends of the truss members are fixed (i.e.,  $k = 2$  in eqn A3), is predicted to occur at 0.98 MPa; this is likely an overestimate, even for elastic buckling, as the ends of the members are likely to be less constrained than the fixed end conditions and any imperfection in the truss further reduces the elastic buckling stress. The interaction between yield and elastic buckling is expected to give rise to plastic buckling at a stress somewhat below that for uniaxial yield in the struts of the truss core. The measured value is consistent with this. The results of the uniaxial compression tests are summarized in Table 2.

### *Plate Bending Under Uniformly Distributed Loading*

The load-deflection curves for the sandwich panels tested in bending under uniformly distributed loading are shown in Fig. 11. Failure was observed to initiate by debonding, with audible cracking of some of the nodes where the truss core is attached to the faces. Debonding events corresponded to sharp dips in the load-deflection curves. Almost immediately following debonding, struts buckled (Fig. 12) and the load continued to increase. As the deflection increased, instances of debonding became more frequent.

The average measured stiffness of the panels was  $1.99 \pm 0.20$  kN/mm, higher than the calculated value of 1.37 kN/mm (eqn A4 [17]). The average initial failure load (corresponding to debonding at the first drop in load) was  $2.05 \pm 0.14$  kN, corresponding to a shear stress in the core of  $0.292 \pm 0.016$  MPa (eqn A6 [18]). The average peak failure load was  $2.65 \pm 0.15$  kN, corresponding to a shear stress in the core of  $0.378 \pm 0.018$  MPa. These shear stresses represent the maximum transverse forces in the plate, occurring at the midpoint of the edges.

The core shear stress required to cause failure by debonding is simply the adhesive strength times the ratio of the area of the bonded node to the area of a unit cell (eqn A7); for the sandwich panels in this study  $\tau_{\text{debonding}}^* = 0.21$  MPa, close to that observed. As with the shear tests, the truss core can fail by uniaxial tensile or compressive yield, elastic Euler buckling or plastic buckling. The predicted uniaxial tensile yield strength  $\tau_{\text{uniaxial yield}}^* = 0.18$  MPa (eqn A8) is slightly lower than the shear stress for debonding. It is possible that there may have been yielding within some of the tensile struts, that was not visible, prior to debonding. Elastic Euler buckling, assuming fixed end conditions, is expected to occur at a core shear stress of 0.69 MPa (eqn A9). After debonding, the degree of end constraint is reduced, so that the core shear stress associated with Euler buckling is expected to be well below this value; the average peak core

shear stress reached in the test was  $0.378 \pm 0.018$  MPa, consistent with an end constraint factor between pinned and fixed (i.e.,  $k = 1.5$ ), as we might expect when some, but not all, of the nodes have debonded. The results of the panel bending tests under uniformly distributed load are summarized in Table 2.

#### *Plate Bending Under Approximately Concentrated Loading*

The load-deflection curves for the sandwich panels tested in bending under an approximately concentrated load are shown in Fig. 13. The average stiffness of the panels was  $0.367 \pm 0.040$  kN/mm, slightly higher than calculated values of 0.34 kN/mm (eqn A10 [17]). The panel failed by debonding, which was initially localized around the loading point at the center of the panel and eventually spread out towards the edges of the panel. The truss lattice exhibited no signs of yielding.

The average initial failure load (corresponding to the first drop in load) was  $0.231 \pm 0.010$  kN. The ultimate failure load was  $0.307 \pm 0.032$  kN. No analysis of the failure load for a pyramidal truss core sandwich panel, simply supported and loaded by an approximately concentrated load, was available for comparison with the experiments. The results of the panel bending tests, with an approximately concentrated load, are summarized in Table 2.

#### *Panel Thermal Conductivity*

The LaserComp testing of a stack of five polystyrene sheets gave a thermal conductivity for the polystyrene of 112 mW/(m·K). However, attempts to minimize contact resistances with thermal paste, according to the LaserComp methodology, were unsuccessful. To calculate the isolated thermal conductivities of the encased aerogel beds, the thermal conductivity and



dimensions of the polystyrene faces and trusses must be known. Since a conclusive value was not able to be obtained experimentally for the polystyrene material, aerogel conductivity values calculated from the LaserComp results are provided for the lowest and highest polystyrene conductivity values found: 112 mW/(m·K) and 150 mW/(m·K). These conductivity values for aerogel can be compared to the expected thermal conductivities based on a separate thermal conductivity test method – known as the hot-wire transient method – as a function of bed density [6]. In the hot-wire method, a fine platinum wire is surrounded by the test material and then a steady electrical current is put through the wire for a short duration; the rate of increase in temperature of the wire (which is dependent on the resistance heating in the wire and the rate of heat dissipation from the wire through the surrounding material) can be used to determine the thermal conductivity of the test material. The hot-wire testing was done with Cabot granules of product number TLD 302 while the LaserComp tests were done using granules of product number P100. A Cabot representative stated that the TLD 302 product is the same as the current P300 product [19]. The P300 product differs from the P100 product only in terms of the particle size range (1.2-4.0 mm versus 0.01-4.0 mm, respectively), otherwise they have the same listed particle densities and thermal conductivity profiles [9]. Additionally, hot-wire testing of the P100 granules provided results similar to the TLD 302 granules. Therefore, these two products were assumed to be comparable for the purposes of this research.

The measurements of the thermal conductivity of the various panel configurations and their aerogel content are listed in Table 3. The discrepancy between the target compression strain and effective compression strain results from the gaps in the compression plate which leave 42% of the panel surface area uncompressed, to avoid crushing the truss structure. For the panels without the truss core, the experimental panel conductivity decreased from 26.7 to 23.4

mW/(m·K) as the compaction of the aerogel increased. For the panels with the truss core, the panel conductivity decreased from 31.9 to 26.9 mW/(m·K) with compaction of the aerogel. The calculated thermal conductivity of the aerogel itself ranged from 22.3 to 19.3 mW/(m·K) in the panels without the truss core and from 25.8 to 21.2 mW/(m·K) in the panels with the truss core (assuming a polystyrene conductivity of 112 mW/(m·K) and that there was uniform density across the aerogel bed). These results are slightly higher than those measured in separate hot-wire tests [6]; this is at least partially due to the additional radiative contribution to heat transfer that is suppressed in the hot-wire tests, which is discussed later in this paper.

The contribution of the adhesive between the truss and face to the thermal conductivity was evaluated by comparing the results for tests in which glue was applied to the entire face and in which glue was applied only at the points of contact between the truss and the face; negligible differences were seen in the results.

## **Discussion**

### *Mechanical Testing*

The use of the truss core sandwich panels gives the proposed aerogel insulation prototype a level of strength and rigidity that makes it a more suitable commercial product than aerogel alone. The compacted granular aerogel has a thermal conductivity of about 19.4 mW/(m·K) (at a compression of 30%). According to the hot-plate conductivity testing, the polystyrene truss adds about 1.5 to 4.6 mW/(m·K) to the overall conductivity of the panels, which is discussed later in this paper. The panels were designed to avoid face failure; the face thicknesses could be reduced to reduce the overall thermal conductivity of the panels.

The shear modulus of the core is well described by previous models [15, 16]. The shear strength is controlled by yielding, followed by debonding of the nodes of the truss from the faces

of the panel; the measured shear strength is lower than predicted from previous models. In uniaxial compression, the truss core fails by plastic buckling, at a stress slightly below the predicted stress for plastic yielding. Elastic buckling is predicted to occur at a stress roughly double that for plastic yielding, assuming fixed-fixed end conditions. The interaction between yield and elastic buckling, as well as imperfections in the truss structure, lead to the observed plastic buckling at a stress below that for yield.

The uniformly loaded bending specimens fail initially by debonding, at a stress very similar to that predicted by the models. However, the models predict that tensile yielding occurs prior to debonding, although no obvious deviation from the elastic modulus is seen in the experiments at the predicted tensile yield stress. This can be explained as follows. Within the truss core, each strut in tension is connected to, and adjacent to, a strut in compression. For polystyrene, the compressive yield strength is more than double that in tension. When the tensile struts initially yield, the compressive struts have not yet reached yield, constraining the tensile struts from substantial plastic deformation.

The stiffness of the approximately point loaded bending specimens was well described by the models [17]. No models were available for the failure stresses of the point loaded specimens.

The mechanical performance of the panels could be improved by optimizing the design of the panel to produce core and face failure at the same load, and by using more sophisticated fabrication techniques, such as plastic injection molding, to create a monolithic truss core sandwich structure to prevent debonding.

### *Thermal Conductivity Testing*

The LaserComp thermal conductivity tests allowed measurement of the contributions from the polystyrene face sheets, the truss core and the aerogel granules to the overall thermal conductivity of the panels. Expected values of each of these contributions came from literature values, theoretical calculations and previous experiments, respectively.

As noted in a previous study, there is a degree of rebound when a bed of granules is compressed and then released. Two tested methods proved to be equally effective in reducing this spring-back phenomenon: holding the bed under compression for an hour and cycling between full and no compressions ten times at a rate of 1 mm/minute. LaserComp test results from panels constructed using each compression method provided similar conductivity results. Consequently, all subsequent panels were made using the cycling method, as this procedure was faster.

During the original development and material selection of the core for the panel system, the truss systems were designed such that they would increase the conductivity of the panel core by no more than 2 mW/(m·K) [20]; in other words, the term  $k'_t$  should not exceed 2 mW/(m·K). Comparing the LaserComp data for the uncompressed panels with and without the truss core (Table 3) and correcting for the slight difference in the bed densities between the two panels, the  $k'_t$  value was 4.6 mW/(m·K) (when comparing the 0% target compression panels with and without a truss), which is over twice the theoretical value. However, when comparing the 15% effective compression panel without the truss core and the 13% effective compression panel with the truss core, this truss contribution factor is calculated to be only 1.5 mW/(m·K). The reason for such a discrepancy between these two comparisons is currently unknown and will require additional testing to definitively determine.

The final comparison provided by the LaserComp data was for the measured conductivity of the aerogel granules. Separate conductivity measurements had been completed on compressed granule beds using the transient hot-wire method; this study found that compacting the bed of aerogel granules decreased the thermal conductivity of the bed until the bed density approached the monolithic aerogel density, at which point the conductivity reached a minimum and then increased with increased compression [6]. One shortcoming of the hot-wire method for silica aerogel is that it underestimates the impacts of radiative heat transfer as compared to other, large scale test methods, such as the steady-state hot-plate method. The reason behind this is that the aerogel is relatively transparent to long-wave radiation for the timescales used in the hot-wire method. It was previously calculated by Cohen that the hot-wire method may underestimate thermal conductivity by as much as  $3.3 \text{ mW}/(\text{m}\cdot\text{K})$  [21]. The calculated aerogel conductivities based on the LaserComp results were all within this margin compared to the expected aerogel conductivities from the hot-wire results except for the uncompressed test panel without the truss, which had LaserComp results lower than the hot-wire expectations. The reason for this unexpected result could not be determined at this time.

One potential source of error in the calculations based on the LaserComp results could be in the manufacturing of the trusses. However, the trusses are currently made with a high precision laser cutter, so the imperfections should be minimal; water displacement measurements were performed on some truss pieces and they were consistently measured to be within 5% of the predicted volume according to the CAD files used to create the trusses. Some of the assumptions made in the theoretical calculation may also need to be reviewed. For example, it was assumed for the purposes of the calculations that heat traveling through the core travels separately through the aerogel and the truss, as if they were completely in parallel with each other. However, in

reality it is likely that some amount of heat traveling through the low-conductivity aerogel would transfer to the relatively high-conductivity truss; this would increase the contribution to conductivity by the truss. This possibility has not been quantitatively reviewed. Future research with this panel system could include a numerical heat flow analysis that more accurately models the panel geometries and 3D heat flows. In actual use, the exterior panel surface could have a convective boundary condition. In that case, the multi-dimensional heat transfer between the truss end and the end plate could be modeled as an annular fin. ISO Standard 6946 – “Building components and building elements. Thermal resistance and thermal transmittance. Calculation method” – could also be utilized to better model the face-to-truss joint. Also, it was assumed that the aerogel granules in the panel were compressed evenly. This is particularly difficult to ensure when the panel contained the truss, which didn’t allow for direct compression of the granules above and below the struts of the truss. An approximate analysis for this situation was done assuming the aerogel value under the shadow of the truss was at its uncompressed state while the balance of the aerogel accounted for the total volume change of the panel. This analysis indicated that it could change the conductivity of the core by less than 1 mW/(m·K) for the compression levels tested by LaserComp.

The conductivity of the aerogel panels used in the LaserComp testing were used for research purposes and were not designed to compete with existing insulation products, though that is the ultimate goal. In order to improve the panel performance, one could use lower-conductivity granules (such as the MIT aerogel granules tested previously [6]) or by sealing the panel and pulling a vacuum. Also, while the truss design has been carefully developed with thermal conductivity in mind, the rest of the panel design could similarly be reviewed for optimal performance.

## **Conclusion**

Analytical and experimental studies were done on the performance of a sandwich panel structure with a pyramidal truss core. A proposed panel prototype was subjected to a uniformly loaded bending, point load bending, uniaxial compression and unidirectional shear, along with thermal conductivity tests. Various theoretical models were examined to determine stiffness, moduli of elasticity and failure modes. The accuracy of these predictions was compared to the experimental results under each load condition. Overall there was fair agreement between the models and the results. The results from the whole-panel thermal conductivity testing were compared to expected values from previous analyses and testing. Again, there was fair agreement between these results and the expected values. Discrepancies were attributed to flaws in assumptions and fabrication. A lightweight structure has been developed which can grant aerogels orders of magnitude more strength while minimally contributing to the thermal conductivity of the material. This research provides validity to the commercial application of aerogels as a competitive building insulation material.

## **Acknowledgements**

We gratefully acknowledge the financial support provided by the DuPont-MIT Alliance and technical discussions with our DuPont liaison, Dr. Vivek Kapur. Mr. Mike Tarkanian, of the Department of Materials Science and Engineering at MIT, provided technical assistance with panel and fixture fabrication and Dr. Nitin Shukla of the Fraunhofer USA Center for Sustainable Energy Systems, Cambridge MA, did the hot plate thermal conductivity measurements; their assistance is greatly appreciated.

## References

- [1] Annual Energy Outlook 2013 Early Release, Washington, DC, 2012.
- [2] L.J. Gibson, M.F. Ashby, Cellular Solids: Structure and Properties, 2nd ed., Cambridge University Press, Cambridge, 1997.
- [3] M.K. Kumaran, A Thermal and Moisture Transport Property Database for Common Building and Insulating Materials: 1018-RP□: Final Report for American Society of Heating, Refrigerating and Air-conditioning Engineers, National Research Council Canada, Ottawa, Ontario, 2002.
- [4] R. Baetens, B.P. Jelle, A. Gustavsen, Energy and Buildings 43 (2011) 761.
- [5] T. Stahl, S. Brunner, M. Zimmermann, K. Ghazi Wakili, Energy and Buildings 44 (2012) 114.
- [6] K. Chen, A. Neugebauer, A. Tang, L.R. Glicksman, L.J. Gibson, Thermal Conductivity of Compacted, Granular Silica Aerogel, 2013. Submitted to Energy & Buildings.
- [7] M.F. Ashby, Materials Selection in Mechanical Design, 3rd ed., Butterworth Heinemann, Oxford, 2005.
- [8] ASTM Standard D638: Standard Test Method for Tensile Properties of Plastics, ASTM International, West Conshohocken, PA, 2010.
- [9] Cabot Aerogel Particles Data Sheet: P100, P200, P300, P400, Boston, MA, 2011.
- [10] K. Finnegan, G. Kooistra, H.N.G. Wadley, V.S. Deshpande, International Journal of Materials Research 98 (2007) 1264.
- [11] Devcon 5 Minute Epoxy Technical Data Sheet, Danvers, MA, 2010.
- [12] ASTM Standard C273/C273M: Test Method for Shear Properties of Sandwich Core Materials, ASTM International, West Conshohocken, PA, 2011.
- [13] M.F. Ashby, D. Cebon, Cambridge Engineering Selector, Granta Design, 1999.
- [14] R.C. Weast, ed., Handbook of Chemistry and Physics, 66th ed., CRC Press, Boca Raton, FL, 1985.
- [15] D.T. Queheillalt, H.N.G. Wadley, Materials & Design 30 (2009) 1966.
- [16] V.S. Deshpande, N.A. Fleck, International Journal of Solids and Structures 38 (2001) 6275.



- [17] D. Zenkert, An Introduction to Sandwich Construction, 1st ed., Engineering Materials Advisory Services, Worcestershire, UK, 1997.
- [18] H.G. Allen, Analysis and Design of Structural Sandwich Panels, 1st ed., Pergamon Press, Oxford, 1969.
- [19] W.P. Lewis (personal correspondence, January 31<sup>st</sup>, 2012).
- [20] T. Goutierre, Advanced Thermal Insulation for Energy Efficient Buildings: Structural Performance of Aerogel Composite Panels, SM Thesis, Department of Mechanical Engineering, Massachusetts Institute of Technology, 2011.
- [21]. E. Cohen and L. Glicksman, Analysis of Transient Hot-Wire Method to Measure Thermal Conductivity of Silica Aerogel, Influence of Wire Length, and Radiation Properties, *ASME J of Heat Transfer* (in press 2014)

Table 1: Panel dimensions.

Panel length, $a$	159 mm
Face thickness, $t_f$	2 mm
Core thickness, $h$	15 mm
Strut thickness, $t$	1.6 mm
Strut width, $w$	1.6 mm
Node width, $b_n$	4 mm
Strut angle, $\omega$	45°
Strut length, $l$	15 mm
Core relative density <sup>1</sup> , $\bar{\rho}$	3.7%

<sup>1</sup> The core relative density was calculated from the SolidWorks file used to cut the trusses and the density of polystyrene.

Table 2: Pyramidal truss core and sandwich plate mechanical test results.

	Measured <sup>1</sup>	Theoretical <sup>2</sup>
<b>Core: Shear</b>		
Shear Modulus (MPa)	$8.32 \pm 1.71$	6.51 (A4d)
0.2% offset shear strength (MPa)	$0.084 \pm 0.007$	
Ultimate shear strength (MPa)	$0.12 \pm 0.01$	0.18 (A8)
<b>Sandwich plate: Uniaxial compression</b>		
Young's modulus (MPa)	$15.1 \pm 0.9$	13 (A1)
Compressive strength (MPa)	$0.50 \pm 0.02$	0.58 (A2) yielding
		0.98 (A3) elastic buckling
		< 0.58 plastic buckling
<b>Sandwich plate: Bending, uniformly distributed load</b>		
Stiffness (kN/mm)	$1.99 \pm 0.20$	1.37 (A4)
Core shear stress; initial failure (MPa)	$0.292 \pm 0.016$	0.18 (A8) tensile yield 0.21 (A7) debonding
Core shear stress; ultimate load (MPa)	$0.378 \pm 0.018$	0.69 (A9) buckling (k = 2) 0.38 (A9) buckling (k = 1.5)
<b>Sandwich plate: Bending, approx. concentrated load</b>		
Stiffness (kN/mm)	$0.367 \pm 0.040$	0.34 (A10)

<sup>1</sup> Measured values are mean  $\pm$  standard deviation.

<sup>2</sup> Brackets refer to the equation number in the Appendix.

Table 3: Thermal conductivity test results for panels with compacted aerogel, with and without the truss core.

	Without Truss Core				With Truss Core		
Panel Target Final Compression	0%	18%	30%	30%	0%	30%	30%
Panel Effective Final Compression	-6%	15%	23%	26%	-11%	13%	13%
Truss Volume Fraction	0%	0%	0%	0%	3.5% <sup>1</sup>	3.4%	3.5%
Compression Method	Settling <sup>2</sup>	Cycling <sup>3</sup>	Holding <sup>4</sup>	Cycling	Settling	Cycling	Cycling
Aerogel Bed Density [kg/m <sup>3</sup> ]	64.2	80.4	88.6	91.3	61.4	78.0	78.0
Conductivity of panel (LaserComp) [mW/(m·K)]	26.7	25.1	23.2	23.4	31.9	26.5	26.9
Conductivity of aerogel bed (LaserComp) [mW/(m·K)] <sup>5</sup>							
-With polystyrene at 112 mW/(m·K)	22.3	20.8	19.3	19.4	25.8	21.0	21.2
-With polystyrene at 150 mW/(m·K)	22.0	20.6	19.1	19.2	24.7	20.1	20.3
Expected conductivity of aerogel bed (hot-wire) [mW/(m·K)] <sup>6</sup>	23.7	20.0	18.5	18.0	24.4	20.6	20.5

<sup>1</sup> Note that the relative density of the core in the panels for mechanical and thermal testing vary lightly due to the different panel dimensions.

<sup>2</sup> "Settling" refers to the uncompressed, naturally settled aerogel granules

<sup>3</sup> "Cycling" refers to cyclic compression used to compact the aerogel

<sup>4</sup> "Holding" refers to a single compression, which was held at the required strain, to compact the aerogel

<sup>5</sup> The "conductivity of aerogel bed" is for the aerogel granules and does not include contributions of the truss.

<sup>6</sup> Using aerogel bed density, expected values were obtained from interpolation of hot-wire data from Chen et al. [6]. These values represent the hot-wire conductivities before any corrections factors have been applied to account for the underestimation in the radiative heat transfer compared to the steady state hot-plate method.

## Appendix I: Mechanics of Truss Core Sandwich Panels

### *Uniaxial Compression*

The properties of the pyramidal truss core, bonded to rigid face sheets and loaded in uniaxial compression, are given by Queheillalt and Wadley [15], who modified the earlier results of Deshpande and Fleck [16] to account for the flattened region at the nodes of the truss core. The Young's modulus is:

$$E^* = E_s \eta \bar{\rho} \sin^4 \omega \quad (A1)$$

Here  $E_s$  is the Young's modulus of the solid from which the core is made,  $\eta = 2l/(2l + b_n)$  is a correction factor to account for the flattened region at the nodes (Fig. 2),  $\bar{\rho}$  is the relative density of the truss core and  $\omega$  is the angle between the inclined truss members and the horizontal plane (Fig. 2).

Assuming that debonding does not occur, the struts in the truss core can fail by plastic yielding, by elastic buckling or by an interaction of the two. Uniaxial yielding of the truss structure occurs at a stress of:

$$\sigma_{pl}^* = \sigma_{ys} \eta \bar{\rho} \sin^2 \omega \quad (A2)$$

Here  $\sigma_{ys}$  is the yield strength of the solid material.

The compressive stress at which elastic buckling occurs is:

$$\sigma_{el}^* = \sigma_{cr} \eta \bar{\rho} \sin^2 \omega \quad (A3a)$$

where

$$\sigma_{cr}^* = \frac{k^2 \pi^2 E_s}{12} \left( \frac{t}{l} \right)^2 \quad (A3b)$$

Here  $k$  is an end constraint factor and  $t$  and  $l$  are defined in Fig. 2. Plastic buckling is expected to occur at a lower stress due to the lower tangent modulus associated with the end of linear elasticity and the onset of plasticity.

### *Sandwich Plate Bending Under Uniformly Distributed Load*

The central deflection of a rectangular sandwich panel, with edge lengths  $a$  and  $b$ , and with isotropic faces and core, under a uniformly distributed load, is given by Allen [18] and Zenkert [17]. The derivation, based on strain energy and the Navier solution for plate bending, assumes thin faces, small deflections and a much greater face stiffness than core stiffness. The total deflection is the sum of the contributions from bending and shearing [17]:

$$w = \beta_1 \frac{qb^4}{D} + \beta_2 \frac{qb^2}{S} \quad (A4a)$$

Here  $q$  is the applied load per unit area,  $D$  is the flexural rigidity, and  $S$  is the equivalent shear rigidity of the core.  $\beta_1$  and  $\beta_2$  are constants that depend on the ratio of the edge lengths,  $a/b$ ; for

the square panels tested in this study, with  $a = b$ ,  $\beta_1 = 4.06 \times 10^{-3}$  and  $\beta_2 = 7.37 \times 10^{-2}$ . The flexural rigidity,  $D$ , is given by:

$$D = \frac{E_f t_f d^2}{2(1 - \nu^2)} \quad (\text{A4b})$$

Here  $E_f$  is the Young's modulus of the face material,  $t_f$  is the thickness of the face,  $d$  is the distance between the centroids of the top and bottom faces and  $\nu$  is the Poisson's ratio of the faces ( $\nu = 0.39$  for polystyrene [13]). The equivalent shear rigidity of the core,  $S$ , is given by:

$$S = \frac{G^* d^2}{h} \quad (\text{A4c})$$

Here  $G^*$  is the shear modulus of the core:

$$G^* = \frac{1}{8} \eta \bar{\rho} E_s \sin^2 \omega \quad (\text{A4d})$$

In sandwich panels, if the faces are thin and stiff relative to the core, then the faces are loaded primarily by normal stresses (eqn A5) while the core is loaded primarily by shear stresses (eqn A6) [18].  $\beta_3$ ,  $\beta_4$ , and  $\beta_5$  are constants that depend on the ratio of the edge lengths,  $a/b$ ; for a square panel ( $a = b$ ):  $\beta_3 = \beta_4 \approx 3.67 \times 10^{-2}$  and  $\beta_5 \approx 0.338$ .

$$\sigma_{\text{faces}} = \frac{qb^2}{dt_f} (\beta_3 + \nu\beta_4) \quad (\text{A5})$$

$$\tau_{\text{core}} = \frac{qb}{d} \beta_5 \quad (\text{A6})$$

The truss cores, loaded in shear, can fail by a number of mechanisms: debonding, uniaxial yield, elastic buckling, and plastic buckling. The shear stress required to fail a pyramidal truss core by all but the first of these mechanisms has been analyzed by Deshpande and Fleck [16], with modifications by Queheillalt and Wadley [15] to account for the flattened nodes.

The shear stress required to give debonding is simply the adhesive strength times the ratio of the contact area at the node to the area of the unit cell:

$$\tau_{\text{debonding}}^* = \tau_a \frac{2wb_n - w^2}{(2l \cos \omega + b_n)^2} \quad (\text{A7})$$

The shear stress required to develop uniaxial yield in the pyramidal truss core (bonded to rigid faces) is [15]:

$$\tau_{\text{uniaxial yield}}^* = \frac{1}{2\sqrt{2}} \sigma_{ys} \eta \bar{\rho} \sin 2\omega \quad (\text{A8})$$

For the polystyrene truss core used in this study,  $\sigma_{ys}$ , is the tensile yield strength, which is less than half the compressive yield strength.

The shear stress required to produce elastic Euler buckling of the compressive struts is [15]:

$$\tau_{\text{buckling}}^* = \frac{1}{2\sqrt{2}} \sigma_{\text{cr}} \eta \bar{\rho} \sin 2\omega \quad (\text{A9a})$$

where

$$\sigma_{\text{cr}} = \frac{k^2 \pi^2 E_s}{12} \left( \frac{t}{l} \right)^2 \quad (\text{A9b})$$

Here  $k$  is again an end constraint factor; we take  $k = 2$ , corresponding to fixed end conditions; in practice, the end constraint is likely to be somewhat less than this value. For plastic buckling, this equation is simply modified by the use of the tangent modulus rather than Young's modulus for the solid.

#### *Plate Bending Under an Approximately Concentrated Load*

Zenkert [17] gives a derivation for the deflection of a simply supported, isotropic, rectangular sandwich panel subject to a concentrated load,  $Q$ , over a small central area of the plate. For a square plate, the central deflection is given by the sum of the bending and shearing deflections ([17], Table 10.1):

$$w = \frac{0.0162 Q b^2}{D} + \frac{0.295 Q}{S} \quad (\text{A10})$$

Here  $D$  is defined in eqn A4b and  $S$  is defined in eqn A4c.

## Appendix II: Methodology for Obtaining Polystyrene Thermal Conductivity

An accurate value for the thermal conductivity of the polystyrene sheets used to make the panel prototypes can be found using the hot-plate method. Since the sheets were too thin to test individually, a thin material test methodology, provided by LaserComp, is used. Multiple tests are performed with stacks with different numbers of sheets. Each test provides a stack resistance represented by the following equation:

$$R_n = \frac{t_n}{k_n} = n \frac{t_p}{k_p} + 2R_{pi} + (n - 1)R_{pp} \quad (A11)$$

Here  $t_n$  is the total thickness of the test stack,  $n$  is the number of sheets in the test stack,  $k_n$  is the thermal conductivity of the stack of  $n$  sheets,  $t_p$  is the thickness of a single sheet,  $k_p$  is the thermal conductivity of the polystyrene sheets,  $R_{pi}$  is the contact resistance between a polystyrene sheet and an instrument plate and  $R_{pp}$  is the contact resistance between successive polystyrene sheets. The measured stack resistances are then plotted as a function of the number of sheets and the slope of the best-fit line,  $\Delta R_n / \Delta n$ , is found. Assuming the contact resistances between the sheets are constant and much smaller than the sheet resistance, eqn A11 can be simplified and rewritten to solve for the polystyrene thermal conductivity:

$$k_p \approx t_p / \left( \frac{\Delta R_n}{\Delta n} \right) \quad (A12)$$

Additionally, in order to minimize the contact resistances, a thin layer of high-conductivity thermal paste should be applied between the sheets.



## Figure Captions

Figure 1: Pyramidal truss structure. (a) Single segment (b) Segments assembled in an orthogonal array.

Figure 2: Unit cell of the pyramidal truss core.

Figure 3: (a) Panel for mechanical testing, without the side walls. (b) Partially fabricated panel for thermal conductivity tests, with double height walls to contain aerogel granules before compaction (one wall removed) (c) Finished panel for thermal testing, with aerogel granules enclosed and with the top face attached.

Figure 4: Schematic of separate one-dimensional heat flow through aerogel and truss core, in parallel.

Figure 5: Schematic of one-dimensional heat flow through stack of polystyrene sheets.

Figure 6a: Uniaxial tensile response of polystyrene.

Figure 6b: Uniaxial compressive response of polystyrene.

Figure 7: Typical shear response of pyramidal truss core.

Figure 8: Fracturing on the tensile struts in a truss core undergoing shearing.

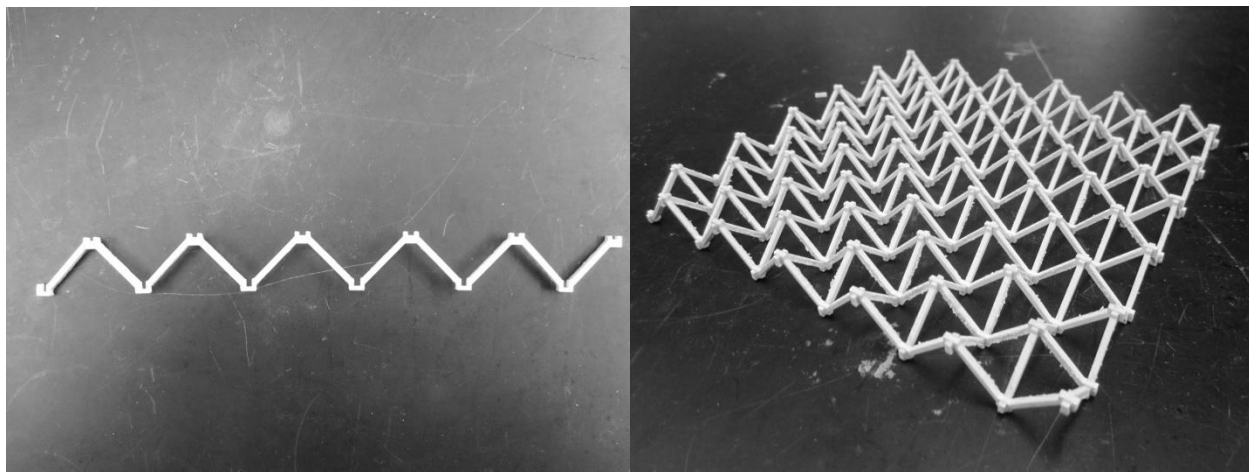
Figure 9: Uniaxial compressive stress-strain curves of the sandwich panels.

Figure 10: (a) Sandwich panel tested in uniaxial compression, showing buckling failure of the struts in the truss core. Buckled struts were permanently deformed. (b) Debonding failure following initial buckling.

Figure 11: Load-deflection curve for a simply supported, uniformly loaded truss core sandwich panel in bending. The core shear stress, calculated from the analysis of Allen [18], is shown on the right hand vertical axis.

Figure 12: Debonding, plastic buckling and cracking on the tensile side of the struts in the truss core of a simply supported, uniformly loaded sandwich panel in bending.

Figure 13: Load-deflection curves for simply supported panels centrally loaded by an approximately point load.



(a)

(b)

Figure 1: Pyramidal truss structure. (a) Single segment (b) Segments assembled in an orthogonal array.

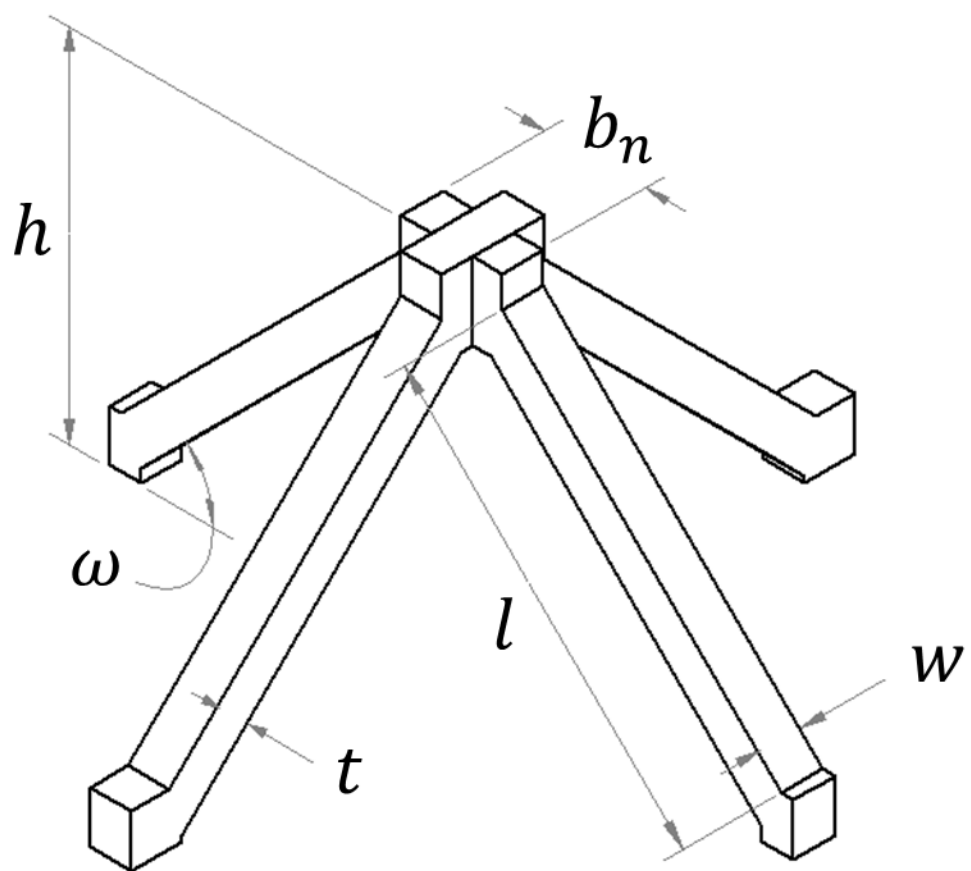
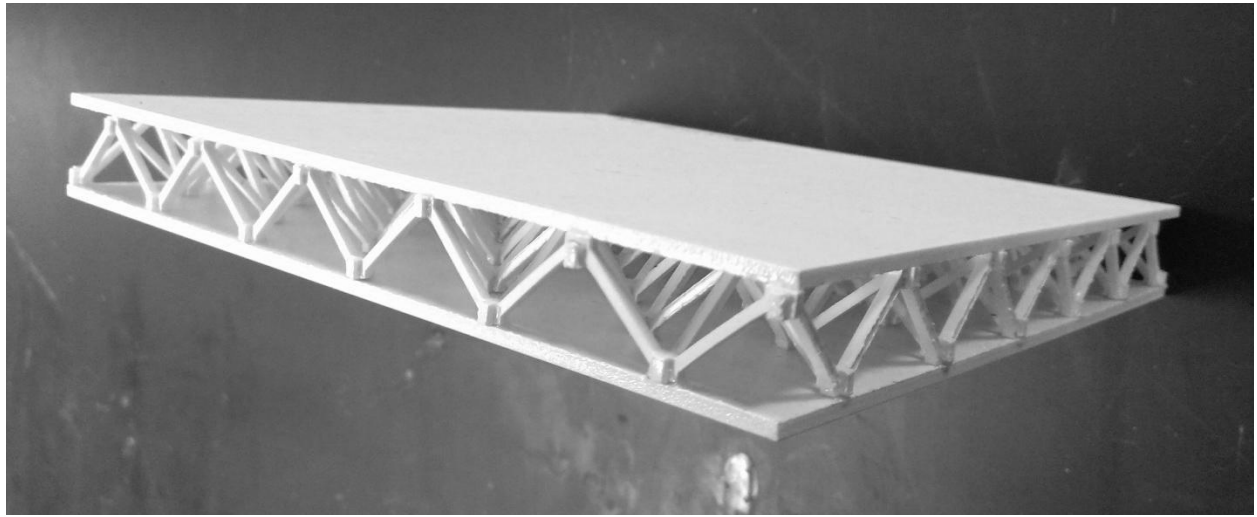
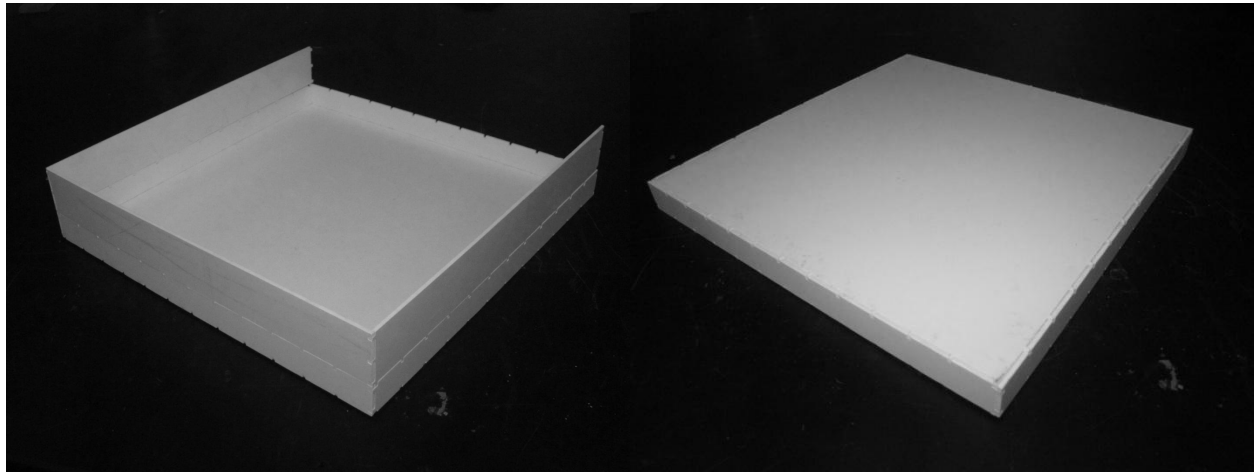


Figure 2: Unit cell of the pyramidal truss core.



(a)



(b)

(c)

Figure 3: (a) Panel for mechanical testing, without the side walls. (b) Partially fabricated panel for thermal conductivity tests, with double height walls to contain aerogel granules before compaction (one wall removed) (c) Finished panel for thermal testing, with aerogel granules enclosed and with the top face attached.

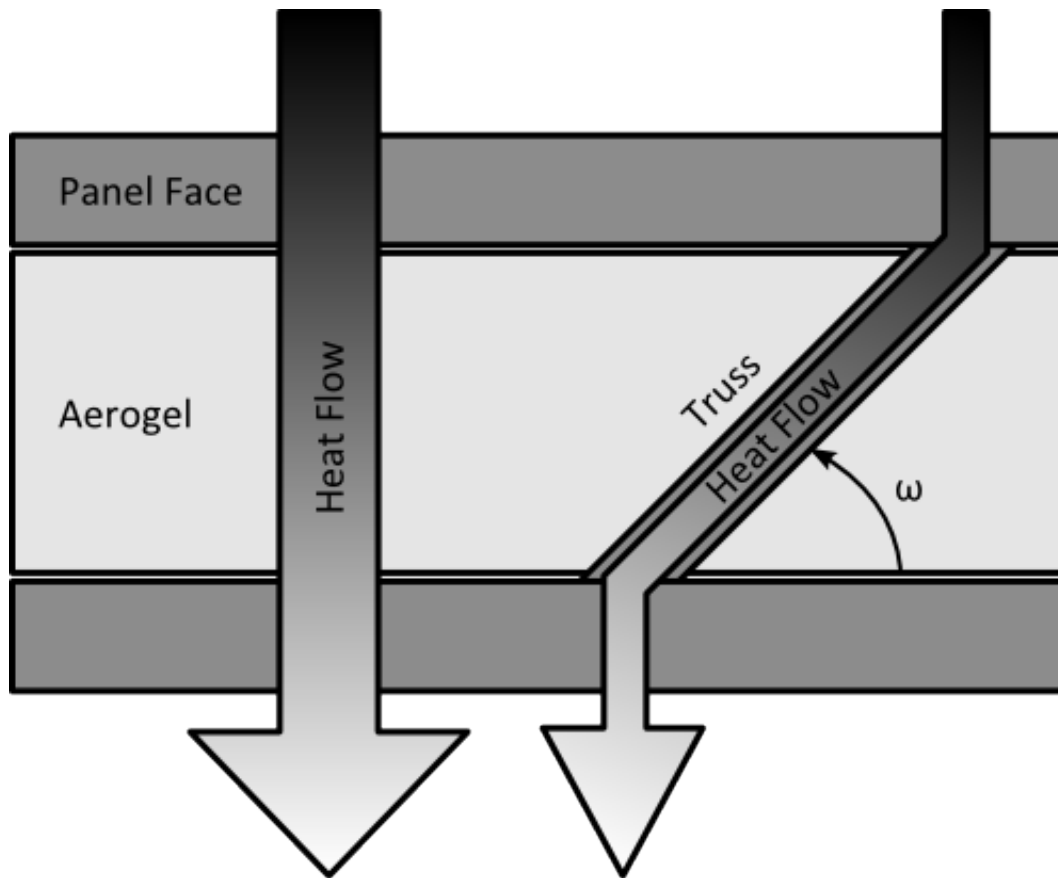


Figure 4: Schematic of separate one-dimensional heat flow through aerogel and truss core, in parallel.

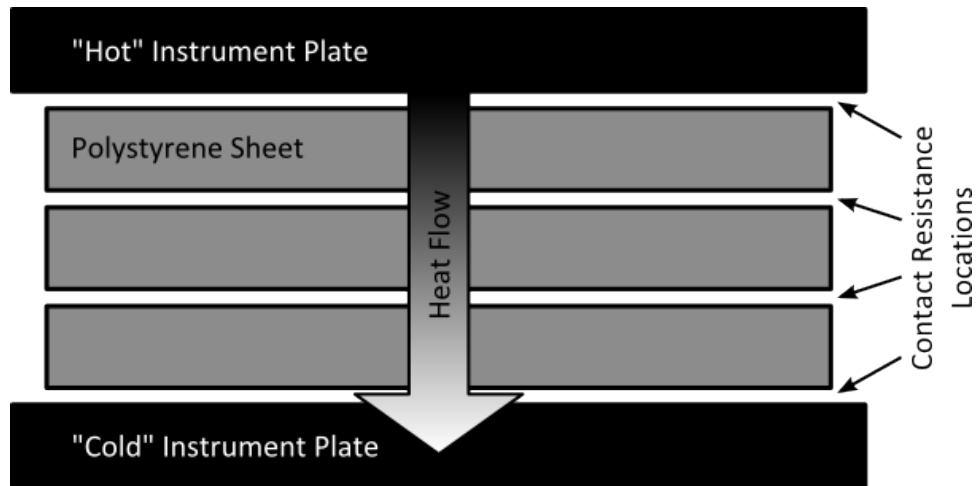


Figure 5: Schematic of one-dimensional heat flow through stack of polystyrene sheets.

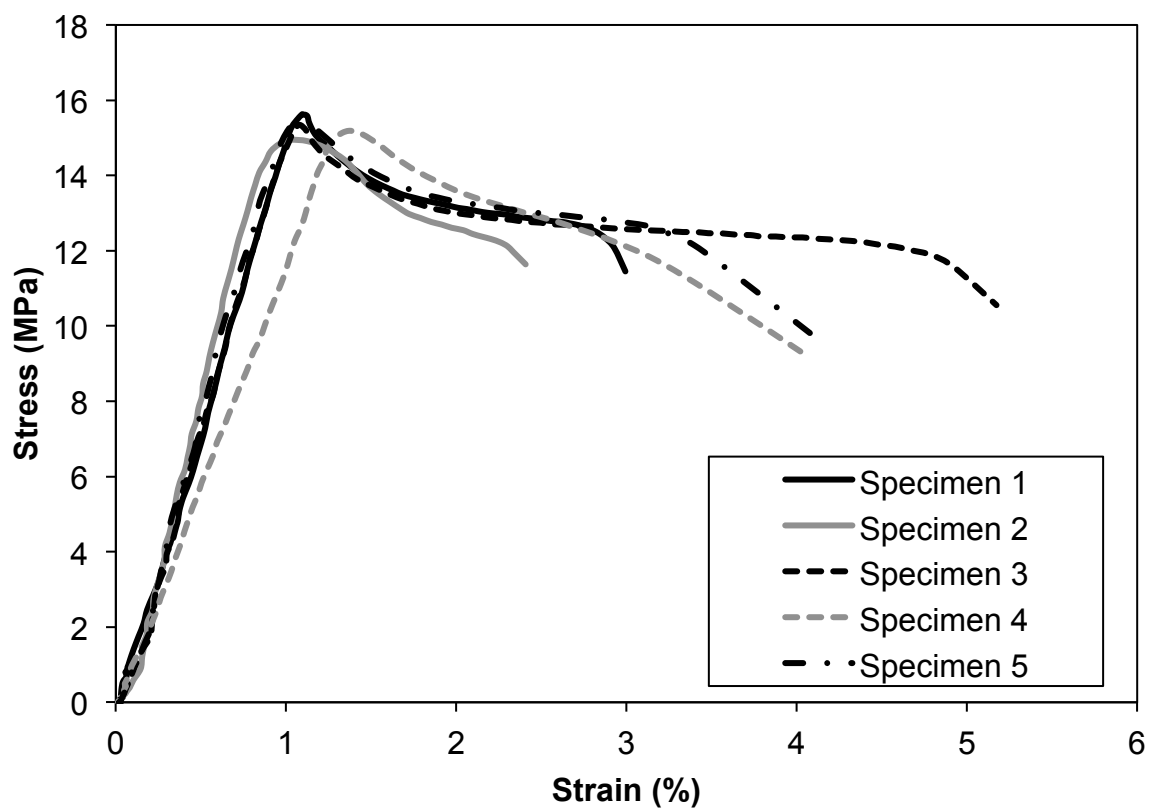


Figure 6a: Uniaxial tensile response of polystyrene.

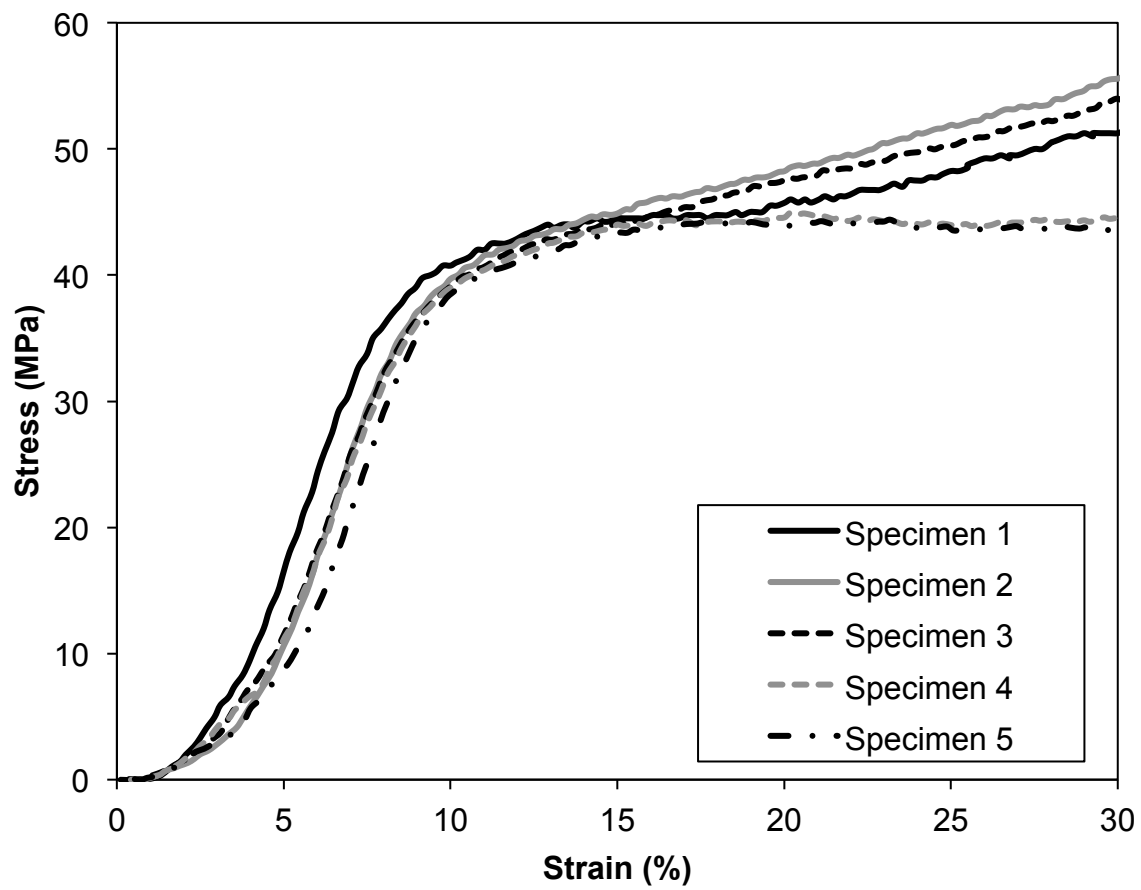


Figure 6b: Uniaxial compressive response of polystyrene.



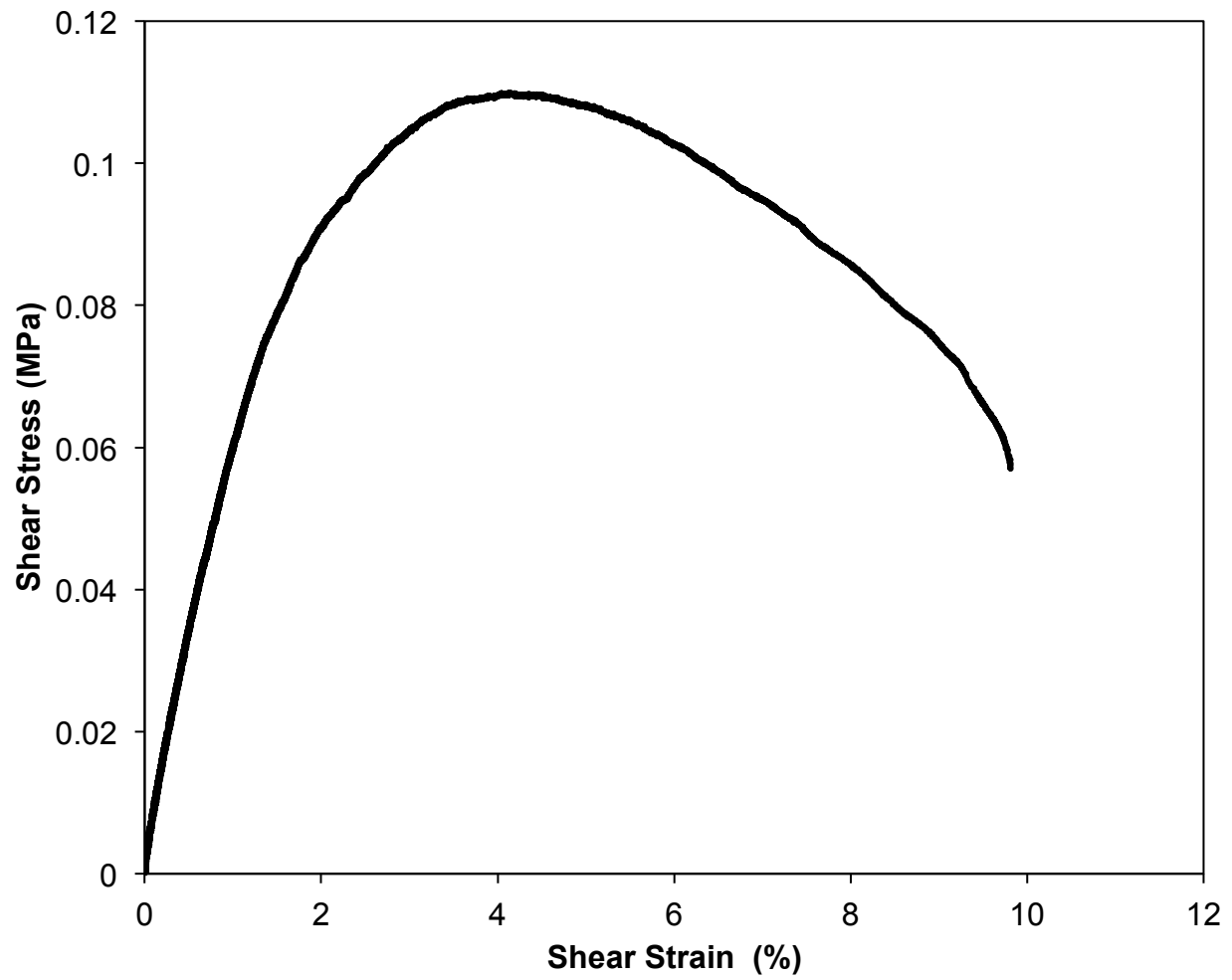


Figure 7: Typical shear response of pyramidal truss core.

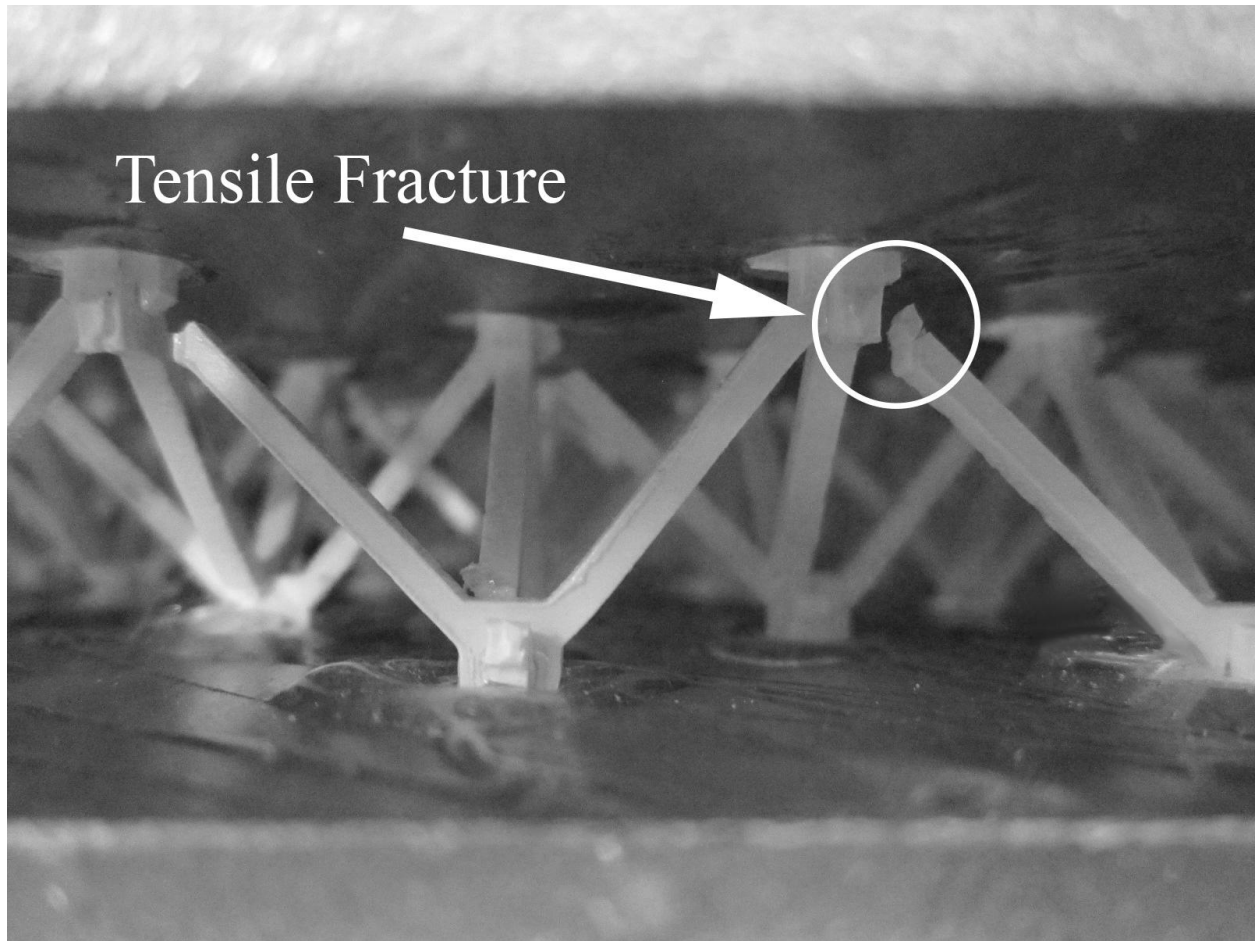


Figure 8: Fracturing on the tensile struts in a truss core undergoing shearing.

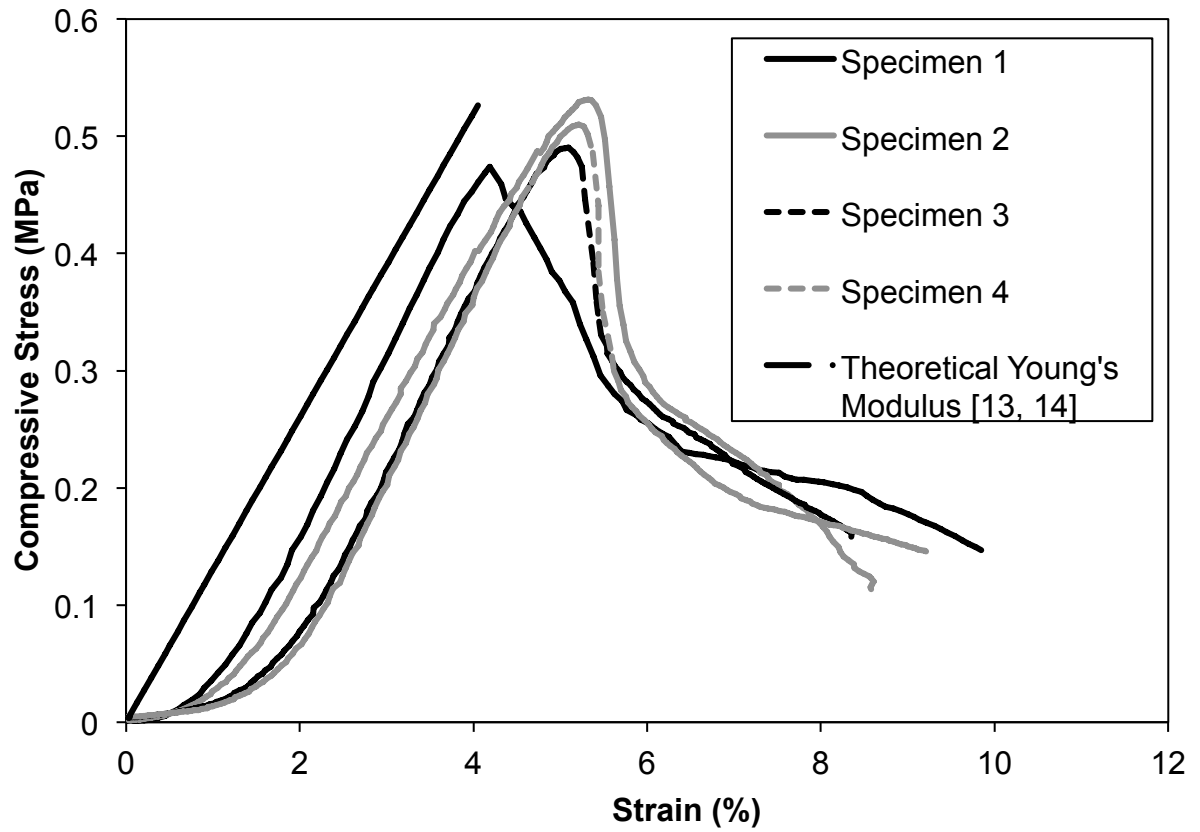


Figure 9: Uniaxial compressive stress-strain curves of the sandwich panels.

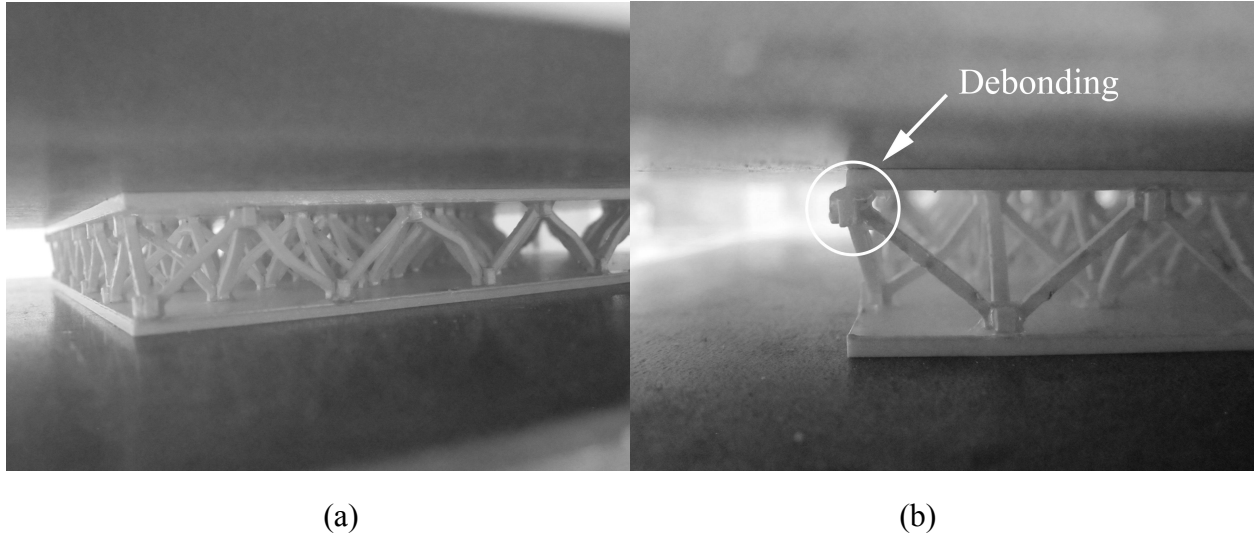


Figure 10: (a) Sandwich panel tested in uniaxial compression, showing buckling failure of the struts in the truss core. Buckled struts were permanently deformed. (b) Debonding failure following initial buckling.

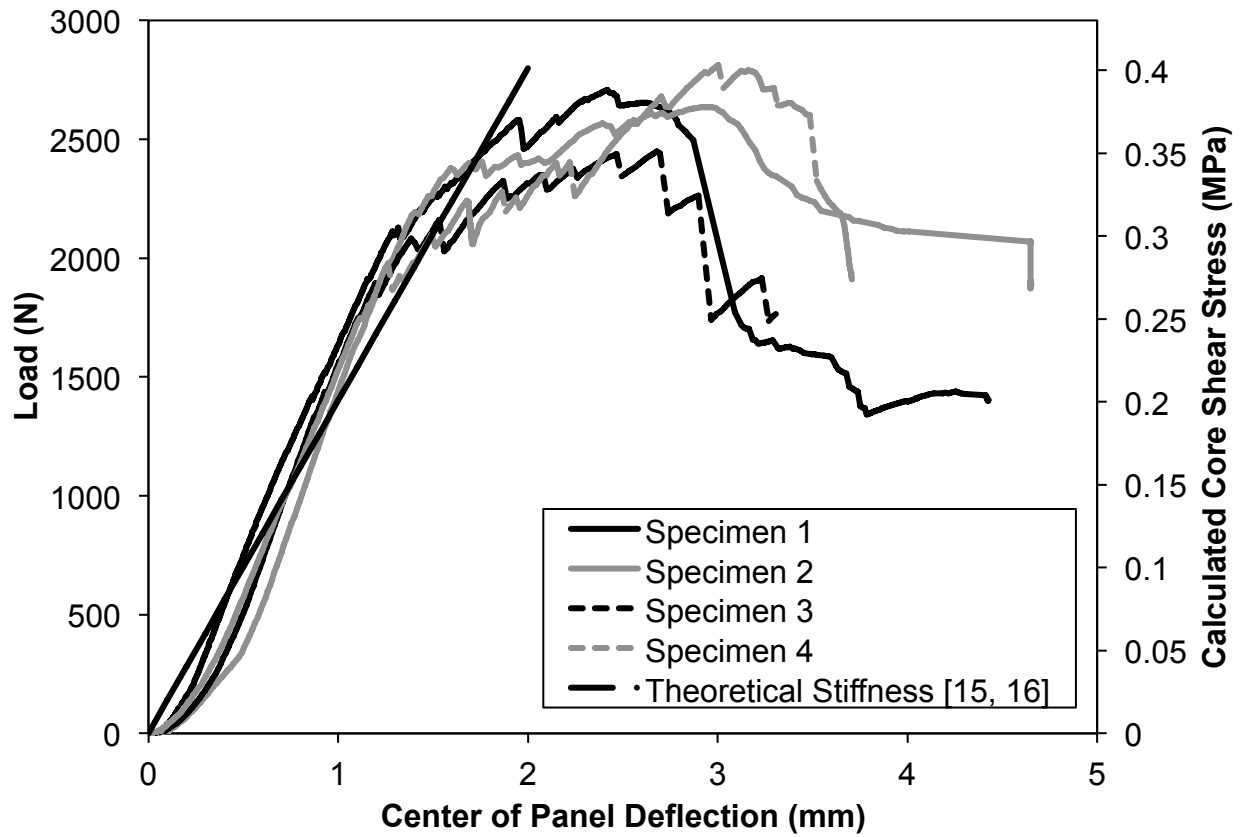


Figure 11: Load-deflection curve for a simply supported, uniformly loaded truss core sandwich panel in bending. The core shear stress, calculated from the analysis of Allen [18], is shown on the right hand vertical axis.

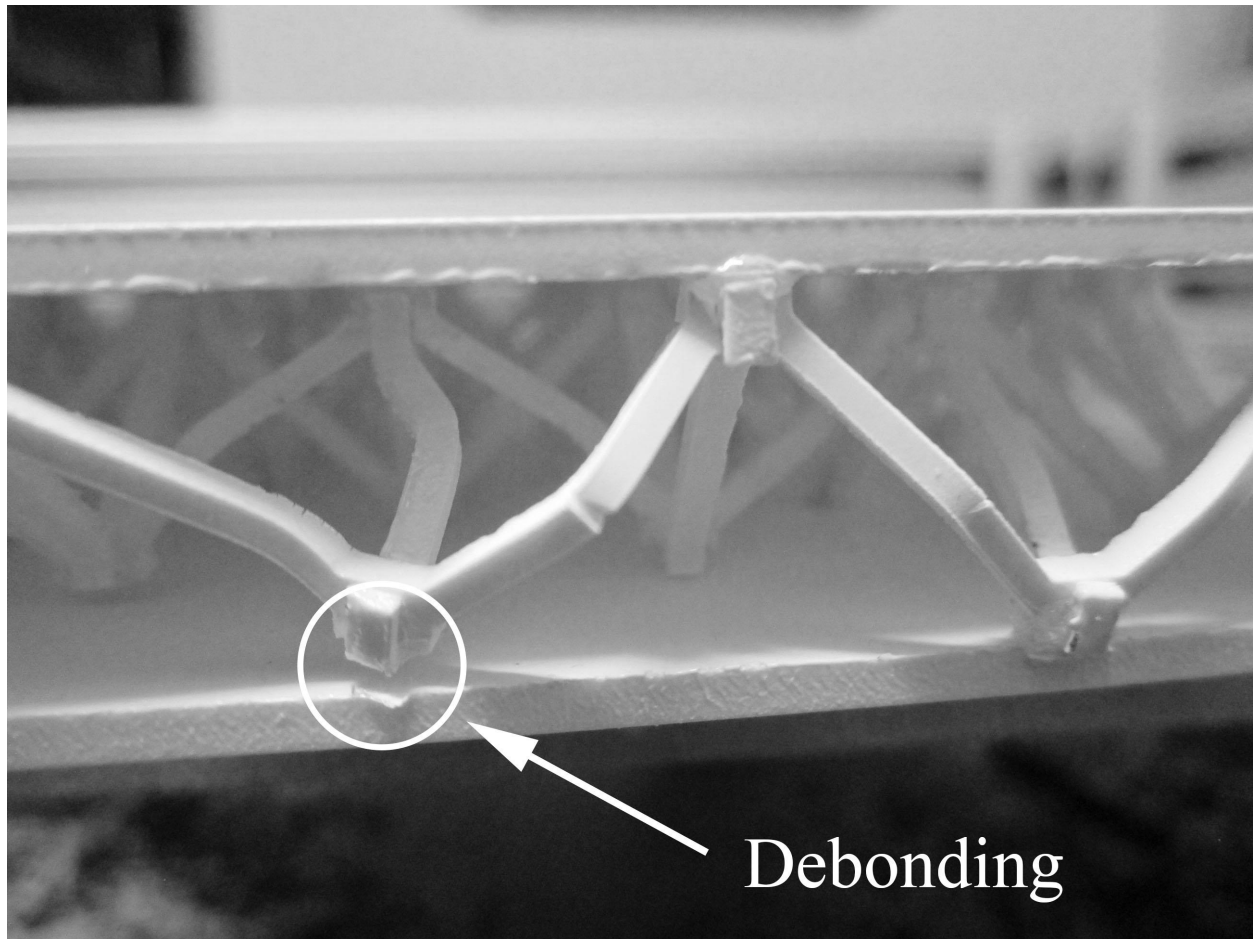


Figure 12: Debonding, plastic buckling and cracking on the tensile side of the struts in the truss core of a simply supported, uniformly loaded sandwich panel in bending.

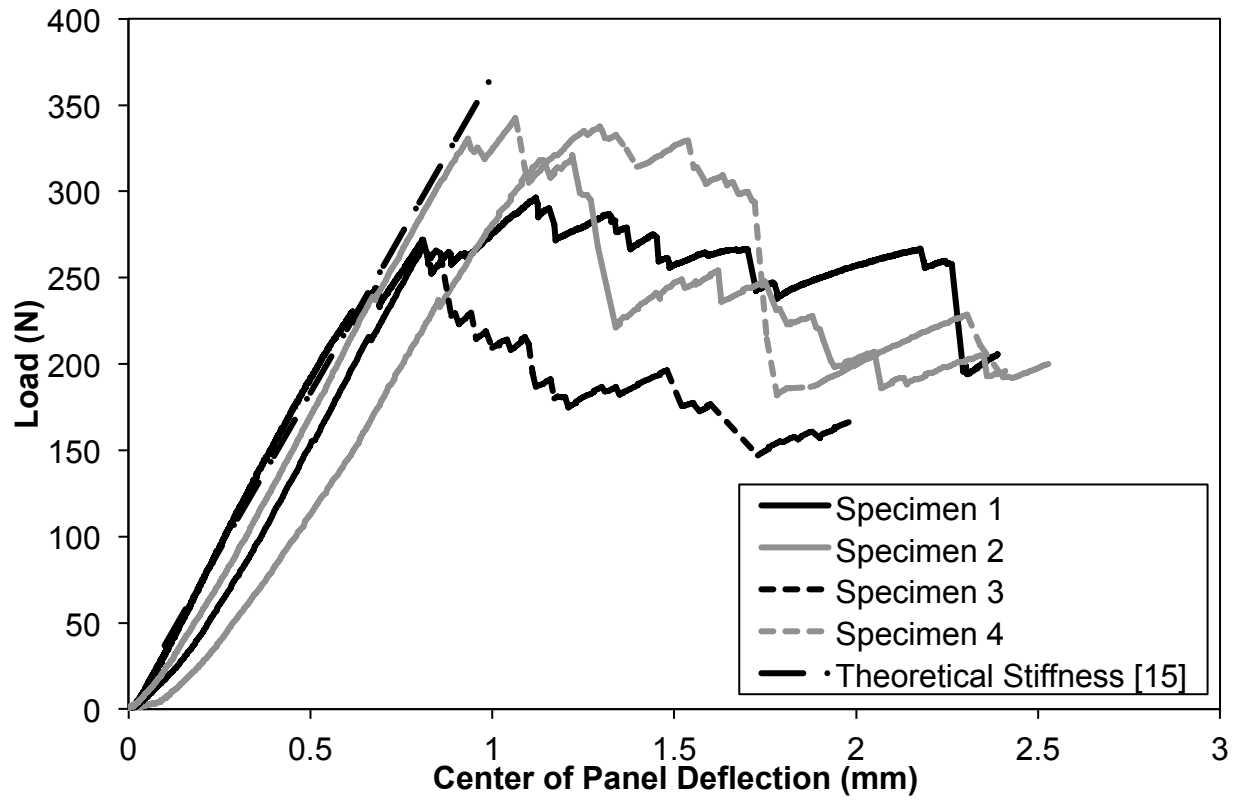


Figure 13: Load-deflection curves for simply supported panels centrally loaded by an approximately point load.